Chapter 11

PICOSECOND SYNCHRONIZATION SYSTEMS FOR QUANTUM NETWORKS

This chapter includes the work published as:

[1] Raju Valivarthi, Lautaro Narváez, Samantha I. Davis, Nikolai Lauk, Cristián Peña, Si Xie, Jason P. Allmaras, Andrew D. Beyer, Boris Korzh, Andrew Mueller, et al. "Picosecond synchronization system for quantum networks." In: Journal of Lightwave Technology 40.23 (2022), pp. 7668–7675.

[1] Keshav Kapoor, Si Xie, Joaquin Chung, Raju Valivarthi, Cristián Peña, Lautaro Narváez, Neil Sinclair, Jason P. Allmaras, Andrew D. Beyer, Samantha I. Davis, et al. "Picosecond synchronization system for the distribution of photon pairs through a fiber link between Fermilab and Argonne National Laboratories." In: IEEE Journal of Quantum Electronics 59.4 (2023), pp. 1–7.

11.1 Introduction

Long-distance quantum networks require distribution of qubits encoded into individual photons. For deployed networks, photons must be transmitted using low-loss, high-bandwidth, and practical channels, such as fiber optics cables. Ideally, photons must also be generated and detected at high rates, for instance using modulated lasers and high-timing resolution (low-timing jitter) nanowire detectors, respectively. The realization of such networks is at odds with environment-induced variations in the length of fiber optics cables. Since photons are identified by recording their times of generation and detection, each with respect to a local (node-based) clock, such variations can lead to misidentification of photons. To avoid this, the variations can be accounted for by adjusting the phases of each local clock based on a centrally located primary clock. This is accomplished by distributing strong optical pulses to the nodes, as conceptualized by the diagram in Fig. 11.1. These pulses can be distributed either separately in parallel fibers or jointly through the same fiber that is carrying the single-photon level quantum signal. This type of clock distribution method, which has been exploited in previous quantum networking demonstrations [1, 2, 3, 4, 5, 6], allows synchronization between all local clocks, and hence identification of photons throughout the network. Importantly, this method enables operation of the network at a high clock-rate and the possibility to perform linear-optic

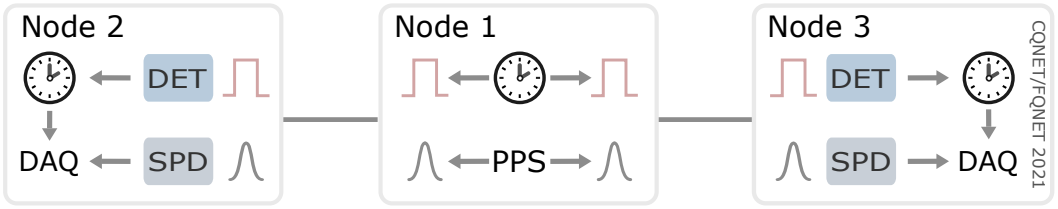

Figure 11.1: Concept of a clock distribution system for a three-node quantum network. A clock is used to generate pulses (top hats) at a central node (node 1) that are distributed to end nodes (nodes 2 and 3) by fiber channels (grey lines) where they are detected (DET) and used to lock the phase of clocks at the end nodes. Simultaneously, light (Gaussians) from a photon pair source (PPS) at the central node is directed into the same fiber towards single photon detectors (SPDs) at the end nodes. Data acqusition (DAQ) systems record the arrival times of the photons with respect to the phase of the clocks at the end nodes, thereby ensuring the clocks are synchronized with the photons.

Bell-state measurements based on two-photon interference, which requires precise synchronization of photons. Using a single fiber for both the clock synchronization and quantum signals makes better use of the limited optical fiber infrastructure that can be employed for quantum communication.

The challenge with this setting is ensuring that the strong optical pulses used for synchronization do not introduce noise that reduces the fidelity of the transmitted qubits. The leading source of noise in optical fiber channels is due to off-resonant Raman scattering of the clock pulses, which produces significantly more red-shifted than blue-shifted light [7]. Typical methods to mitigate this involve strong temporal and spectral filtering [8] or using photons that are significantly blue shifted from the clock pulses [1]. Accordingly, there is little work to investigate the role of the Raman noise when photons are red-shifted from the clock pulses and both are in the same fiber, in particular if the photons and the clock pulses are at wavelengths within the standard fiber telecommunication windows, and if such noise prohibits reaching ps-scale timing resolution of the clock distribution system.

In Section 11.2, we develop a picosecond-level clock synchronization system at Caltech and demonstrate entanglement distribution over optical fiber alongside a coexisting classical channel for optical clock distribution. We characterize the effect of noise sources, such as Raman scattering and dark counts, on the fidelity of transmitted entangled qubits over the network. In Section 11.3, we deploy the system

in a real-world fiber network with remote nodes at Fermi National Accelerator Laboratory (FNAL) and Argonne National Laboratory (ANL). We demonstrate, for the first time, picosecond-scale clock synchronization between national laboratories over metropolitan distances, achieving 2 ps synchronization of remote nodes at FNAL and ANL. This work is a crucial step for implementing advanced entanglement-based protocols, such as MDI-QKD and quantum repeaters, across metropolitan regions for the proposed quantum internet connecting DOE laboratories [9].

11.2 Picosecond synchronization system

First, we demonstrate a three-node, all-fiber, quantum network at the CQNET site (see Sec. 7.2 in Chapter 7) that is supported by a low-noise, scalable, and automated clock distribution system. This is realized by distributing photon pairs in the telecommunication C-band (1.5 μm) simultaneously with strong optical "clock" pulses in the telecommunication O-band (1.3 μm) in the same fiber. Specifically, light is distributed from a central node over two 11 km-length fibers to two end nodes. The pulses used for clock distribution are created by bias switching a laser diode whereas the pulses generating the photon pairs through spontaneous parametric down-conversion (SPDC) are carved from a continuous-wave laser by a Mach-Zehnder modulator. Our setup uses in-house, high-bandwidth, and scalable electronics to generate 3.7 V (peak-to-peak) pulses having near-Gaussian distributions with durations as low as 47 ps and sub-ps timing jitter. We quantify the effect of Raman scattering by measuring the coincidence-to-accidental ratio (CAR) of the distributed photon pairs using a free-running data acquisition and control system. We find that the clock distribution system reduces the CAR from 77 ± 14 to 42 ± 2, which is still sufficient for high-fidelity qubit distribution. Furthermore, we observe only 2 ps of timing jitter (over 1 minute of integration) between clocks at the central and end nodes, suggesting our method can be used for high-rate networks.

Experimental setup

Our three-node quantum network and corresponding synchronization system is schematized in Fig. 11.2 and, other than the custom electronics and single-photon detectors, consists of fiber-based and off-the-shelf components. The central node consists of a photon pair source (PPS) operating at the telecommunication C-band wavelength of 1536 nm and two transmitters (Tx1, Tx2) generating clock pulses at the telecommunication O-band wavelength of 1310 nm. By way of wavelength division multiplexer/demultiplexers (MUX/DEMUXs), the clock pulses and single

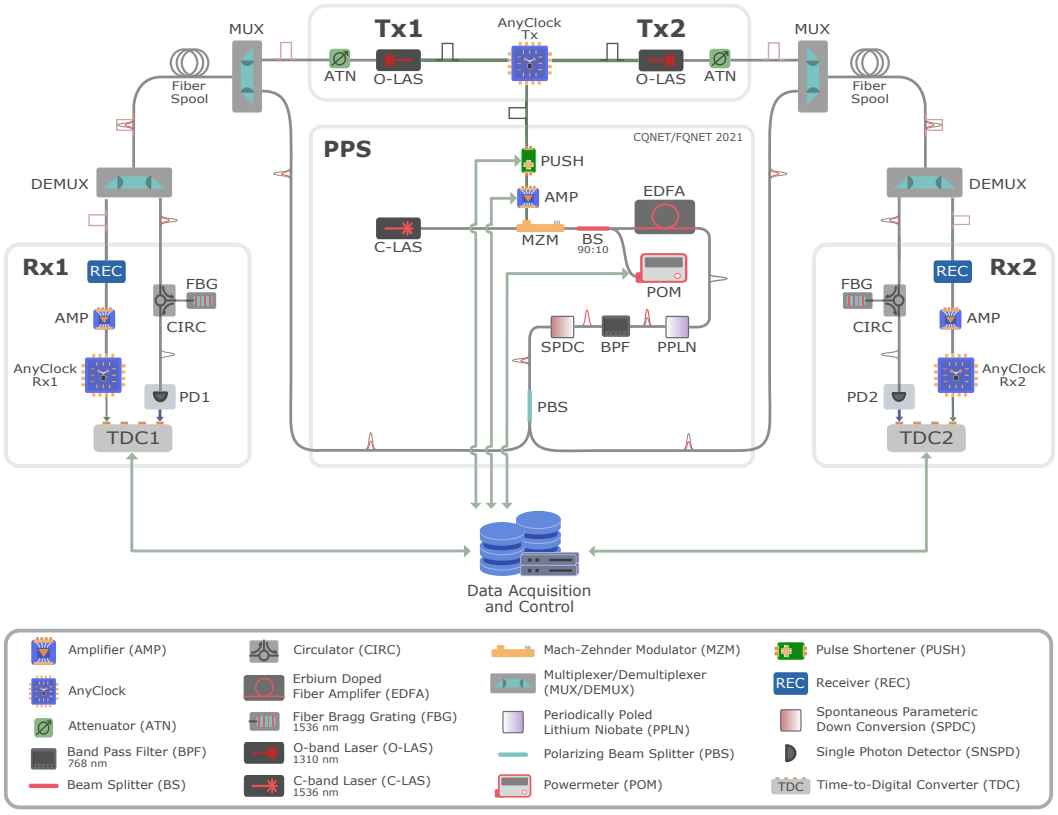

Figure 11.2: Schematic of fiber-based three-node quantum network and synchronization system at Caltech. See main text for description. Clock pulses are indicated by top hats whereas grey and red Gaussian-shaped pulses indicate light of 1536 nm and 768 nm wavelength, respectively. The loss contributions from each fiber spool is 2.26 dB and 2.8 dB, respectively, whereas each WDM and FBG adds 2 dB and 6 dB of loss, respectively.

photons are directed into fibers and distributed to end nodes via 11 km-length spools of single-mode fiber. At the end nodes, the clock pulses and photon pairs are separated using DEMUXs and subsequently detected (Rx1, Rx2). As described in detail below, we ensure the photon pair generation and detection events are synchronized by (i) generating a photon pair synchronously with a clock pulse and (ii) recording the time between the detection of the clock pulse and the individual photon at each end node.

Clock distribution is seeded by a 200 MHz voltage oscillator (AnyClockTx) at the central node. It generates 2.5 ns-duration pulses that are used to bias switch two O-band laser diodes (O-LASs), generating optical clock pulses of similar du-

ration which are subsequently attenuated to an average power of 0.25 mW. This setup is indicated by Tx1 and Tx2 in Fig. 11.2. Synchronous with the optical clock pulse generation, AnyClockTx creates a third pulse which is shortened to a duration as low as 47 ps (PUSH) and power-amplified by up to 28 dB (AMP) using customized electronics, then directed to a 20 GHz-bandwidth fiber-coupled Mach-Zehnder modulator (MZM) within the PPS setup. The pulse amplitudes approximately correspond to the π-voltage of the MZM. The PPS setup contains a C-band laser (C-LAS) emitting continuous-wave light of 1536 nm wavelength that is modulated using the MZM to create 74 ps-duration optical pulses with an extinction ratio of 28 dB at a (clock-synchronized) repetition rate of 200 MHz. After passing a 90:10 beam splitter used for monitoring (POM) the stability of the MZM, these pulses are amplified by an erbium-doped fiber amplifier (EDFA), producing pulses with average power of 100 mW, and then directed to a fiber-packaged periodically poled lithium niobate (PPLN) waveguide which up-converts the light to 768 nm wavelength. Next, residual 1536 nm light is removed using a band-pass filter (BPS) and the pulses are directed to a second PPLN waveguide configured to produce 1536 nm-wavelength photon pairs by Type-II SPDC. A fiber-based polarizing beam splitter (PBS) separates each photon from the pair into different fibers, where they are each directed to the MUXs, and combined with the optical clock pulses in the fiber spools.

At the end nodes, after passing the DEMUXs, the individual photons are filtered by fiber Bragg gratings (FBGs), by way of circulators (CIRC), to a bandwidth of 2.5 GHz and detected using cryogenically cooled superconducting nanowire single photon detectors (SNSPDs) with 50 ps timing jitter (PD1 and PD2). The electrical pulses generated by the SNSPDs are directed to time-to-digital converters (TDC1, TDC2). The optical clock pulses are received by 200 MHz-bandwidth amplified photodiodes (REC) which generate electrical pulses that are amplified (AMP) by 15 dB using scalable custom electronics. These pulses adjust the phase of 200 MHz voltage oscillators (AnyClockRx1, AnyClockRx2) at the end nodes which produce pulses that are detected by the TDCs. The TDCs then record the time difference between the electrical pulses generated by the SNSPDs and the oscillators to verify the synchronization. This time difference is logged using a scalable data acquisition and monitoring system (indicated in Fig. 11.2) that enables uninterrupted quantum networking for an extended time duration (>days).

Scalable and high-bandwidth custom electronics

Pulsed quantum networking experiments typically use either mode-locked lasers [3] or laser diodes and modulators, such as MZMs, driven by electrical pulses generated from arbitrary waveform generators [10] and off-the-shelf multi-purpose amplifiers [11] (see Chapters 8 and 10). These approaches are expensive, bulky, and not scalable to multi-node quantum networks. We address this shortcoming by in-house developing custom pulse (duration) shorteners and amplifiers, referred to as Picoshort and Picoamp modules, respectively, that shape electrical pulses from the AnyClockTx oscillator. The resulting pulses are used to drive the MZM to its π-voltage, producing high-extinction pulses (>20 dB) for the PPS. Short-duration (<100 ps) pulses allow the possibility of measuring high signal-to-noise ratios, the ability to create time-bin qubits in a single clock event (by splitting the pulse into two), and the realization of photon pairs with high spectral purity. We also use a Picoamp to increase the output voltage of the REC photodiodes for compatibility with the AnyClockRx oscillators.

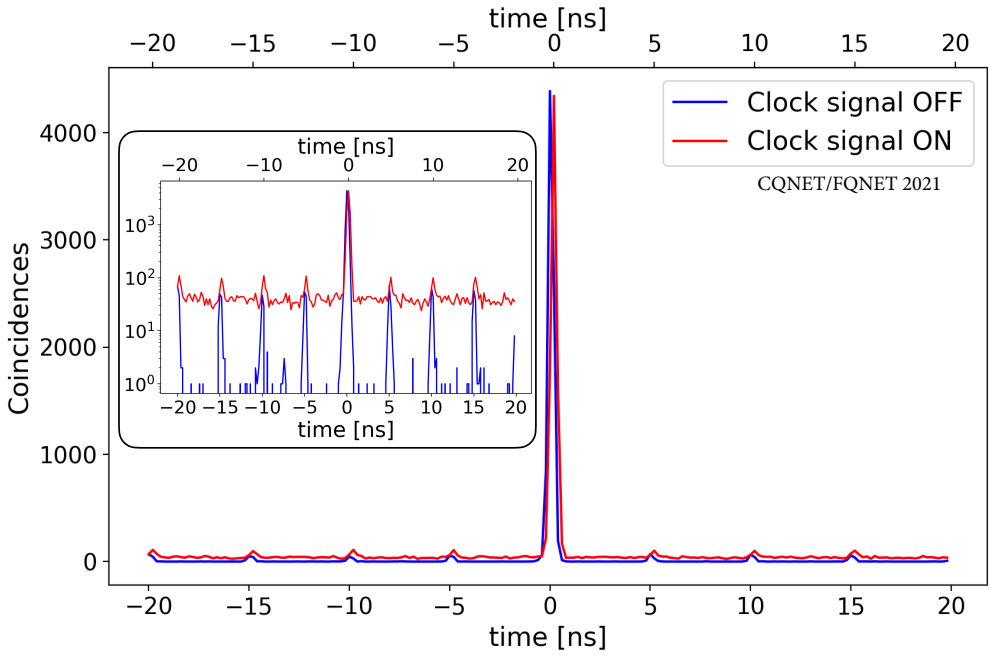

Figure 11.3: Coincidence histogram with the clock distribution enabled and disabled. The small time delay between the two histograms is due a small difference in trigger voltage threshold. Inset: Coincidence histogram with a log vertical scale reveals the Raman noise from the clock pulses.

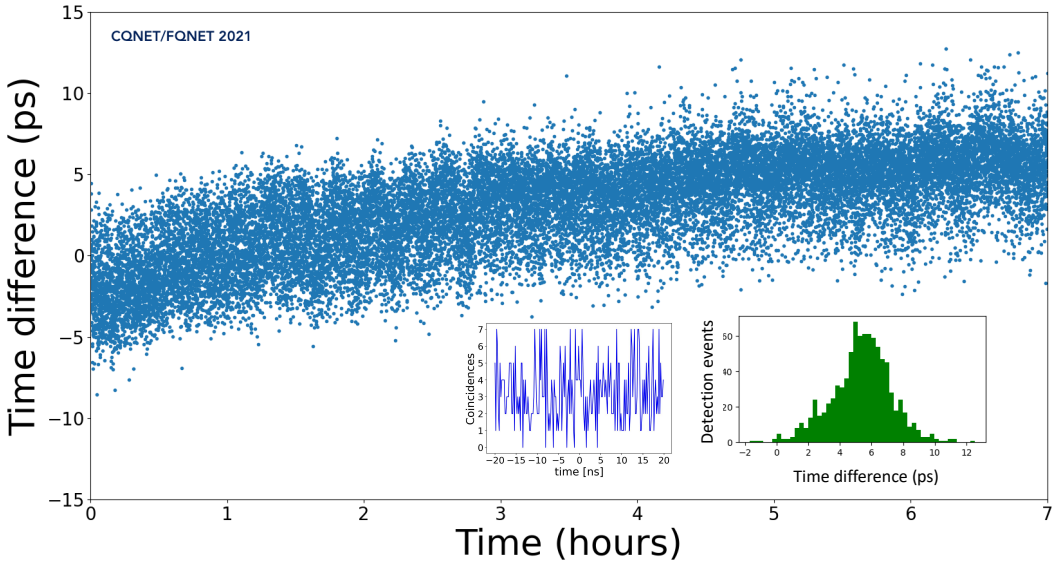

Figure 11.4: Variation of the time difference between the arrival of clock pulses at Rx1 and Rx2 over 7 h. The maximum time difference is 5 ps due to fiber length variations. Inset (left): histogram of photon pair correlations without the clock system enabled. Inset (right): histogram of the time difference over a 900 s time scale indicates a timing jitter of 2 ps.

Results

We characterize our quantum network setup by distributing photon pairs both with and without the clock distribution enabled, and measure the effect of the Raman noise from the clock pulses. The role of noise is captured by the CAR of the photon pairs, $CAR = C/A$, where, in the absence of noise, C corresponds to the coincidence detection rate of photons originating from the same event, whereas A corresponds to the coincidence detection rate of photons originating from different events. Note that in this context, the CAR is equivalent to the cross-correlation function $g^{(2)}$ [12]. Dark counts and Raman scattering can reduce CAR as a noise detection event may be recorded instead of a photon. Our method is well-suited for quantum networks as channel loss ensures accidental coincidences. Our PPS produces a pair with a probability of 1% ($\sim 1/CAR$ as measured at the output of the PPS) per pulse [13]. Channel loss, calculated by taking the ratio of the coincidence rates to the single photon detection rates [13], from PPLN waveguide to the SNSPDs are 24 dB and 26 dB, which are equivalent to ~120 km and ~130 km lengths of single-mode fiber, respectively. We measure the arrival time difference of SNSPD detection events at Rx1 and Rx2 over 5 minutes, both with and without the clock pulses, compiling all

events into histograms, see Fig. 11.3. We sum the detection events over a 200 ps interval around the peak at zero time delay to calculate coincidences (C), whereas the average number of detection events in a 200 ps interval around each of the accidental peaks is used to determine the accidentals (A). The measurements yield a CAR of 77 ± 12 without, and a CAR of 42 ± 2 with, the clock distribution enabled, respectively, which are both well above the classical limit of $CAR = 2$. To place our results into context for qubit distribution, if these photon pairs were to be time-bin entangled, e.g. using the approach demonstrated in Chapters 8 and 10, and if no other imperfections play a role, the measured reduction of CAR from the Raman noise suggests a reduction of fidelity $CAR/(CAR + 1)$ [14] from 99% to 98% or the same reduction in the entanglement visibility $(CAR - 1)/(CAR + 1)$ [15]. This visibility is well-above the $1/3$ required for non-separability of a Werner state [16] and the non-locality bound of $1/\sqrt{2}$ [17]. Thus, the noise introduced by our clock distribution system plays a minimal role in our quantum network.

Importantly, we also determine the timing jitter of our clock distribution method, which sets an upper-bound on the rate of the quantum network. To compare the arrival time of the clock pulses at Rx1 and Rx2 (after the AnyClockRx1 and AnyClockRx2 oscillators), we use an oscilloscope to measure a timing jitter of 2 ps over a timescale of 60 s, and a time difference that slowly drifts by 5 ps over 7 h owing to fiber length variations, see Fig. 11.4. Note that we use an oscilloscope because the current configuration of the TDC adds up to 7 ps timing jitter, but with a standard upgrade this can be as low as 3 ps [18]. Since the clock pulses are attenuated to ensure a minimal reduction in CAR, our measurement is limited by the noise floor of detectors only. Nevertheless, the timing jitter of our clock distribution currently sets an upper-bound on our distribution rate of $\sim$ 300 MHz, which is sufficient for quantum networks spanning a few hundred kilometers, that is, metro-scale or inter-city networks. Note that we have also measured the coincidence histogram of the photon pairs without the synchronization system enabled, finding only classically correlated noise (see inset of Fig. 11.4), further showing the necessity of our synchronization system.

11.3 Deployment in a real-world network

Next, we present a demonstration of picosecond-scale synchronization of C-band photon pairs over deployed fiber optic cables connecting three remote nodes by distributing the clock pulses in either the telecommunication standard O- or L-bands. A map of the three-node quantum network is shown in Fig. 11.5 along with

the approximate paths of the optical fiber links between the nodes. Two of the nodes are located in the Fermi National Accelerator Laboratory (FNAL) FQNET/IEQNET site (see Sec. 7.2 in Chapter 7). These include the central node at the Feynman Computing Center (FNAL-FCC) and one of the end nodes at the D0 Assembly Building (FNAL-DAB), and are stationed 2 km apart. The third node is located at the Argonne National Laboratory (ANL) IEQNET site, and is 57 km away from FNAL-FCC. Each of these nodes are connected with pairs of fibers. The central node at FNAL-FCC contains a photon pair source as well as a commercial all-optical telecom switch from Polatis and the end nodes at FNAL-DAB and ANL contain the superconducting nanowire single photon detectors (SNSPDs). The quantum-correlated photon pairs are split, and each photon in the pair is sent into one of these 2 km-2 km and 57 km-57 km fiber pairs linking the nodes, corresponding to total transmission distances of the quantum states of 4 km and 114 km, with 2 km and 57 km of shared quantum-classical coexistence with a clock signal.

Finally, we measure the noise introduced to the quantum information due to quantum-classical coexistence signals distributed between nodes in our network and find that in the FNAL-FCC to ANL link, the O- and L-band clocks reduce the coincidence-to-accidental ratios (CAR) from 51 ± 2 to 5.3 ± 0.4 and 2.6 ± 0.3, respectively. These measurements demonstrate that our research prototype network is suitable for point-to-point schemes and for two-photon interference-based teleportation protocols, representing a notable milestone towards establishing a national research quantum internet between the U.S. Department of Energy laboratories as envisioned in DOE's blueprint for the quantum internet [9].

Experimental setup

Our photon pair source is situated at FNAL-FCC. Using a commercial arbitrary waveform generator (AWG), short radio-frequency (RF) pulses with widths of 80 ps and separated by 5 ns are generated, amplified, and used as the input to a fiber-coupled Mach-Zehnder Modulator (MZM) [10, 19]. Light at 1536 nm wavelength produced by a continuous wave fiber-coupled laser is directed into the MZM to produce pulsed light. The pulsed light is directed into an erbium-doped fiber amplifier (EDFA) and then sent through a periodically poled lithium niobate (PPLN) waveguide to upconvert the 1536 nm light to 768 nm. A band-pass filter is used to remove any residual 1536 nm light. A second PPLN waveguide takes the 768 nm light as input to produce time-correlated photon pairs at the original wavelength of 1536 nm through Type-II spontaneous parametric down conversion process (SPDC). A fiber-

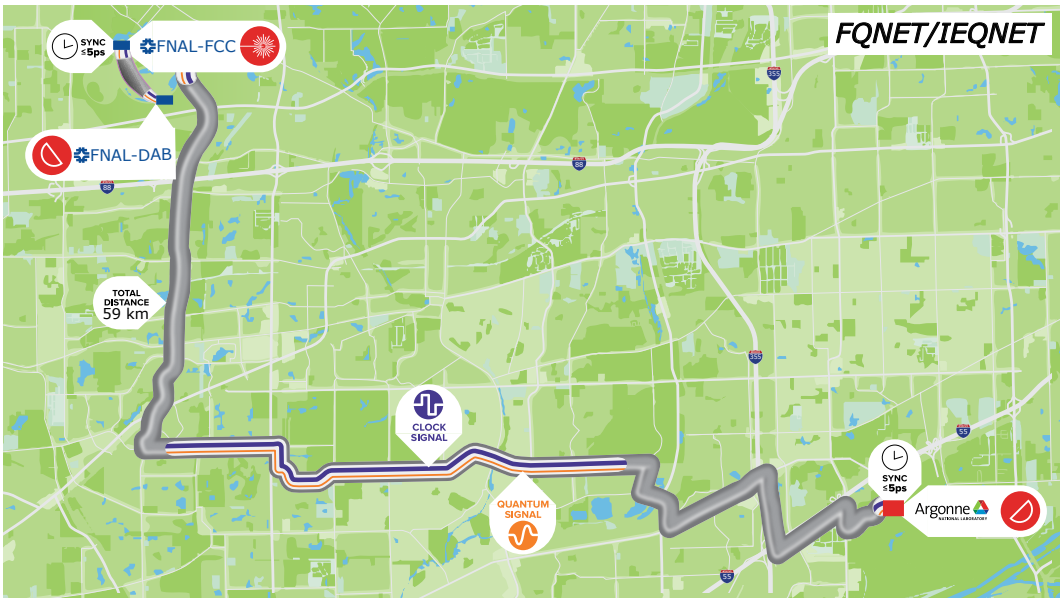

Figure 11.5: This image depicts the separation of the nodes in our real-world network. FNAL-FCC and FNAL-DAB are connected with 2 km of dark fiber and FNAL-FCC and ANL are connected with 57 km of dark fiber. We keep our master clock at FNAL-FCC, and distribute the signal to FNAL-DAB and ANL, choosing the path via an optical switch located at FNAL-FCC. The FNAL nodes are depicted by the blue rectangles and the ANL node is depicted by the red rectangle.

based polarizing beam splitter separates the photon pair into individual photons, one of which is directed to a dense wavelength division multiplexer (DWDM) and multiplexed with the clock signals described in the next subsection. The multiplexed quantum and classical channels are sent to the optical switch located at FNAL-FCC, which routes their path to FNAL-DAB or ANL. The other photon of the pair is sent directly, using a dedicated fiber, to the optical switch and routed to the same node.

At the FNAL-DAB and ANL nodes, the combined quantum and clock channels are sent through a DWDM de-multiplexer (DEMUX) to separate them. The quantum channel is filtered by two or three additional DEMUX's and then a 4 GHz bandwidth fiber Bragg grating (FBG) filter to isolate the 1536 nm quantum frequency channel to within a wavelength of 0.03 nm. These filters reduce the effects of dispersion and improves the indistinguishability of the photons. The FNAL-DAB and ANL nodes are equipped with two superconducting nanowire single photon detectors (SNSPD) to detect the incoming photons with timing jitter (resolution) of less than 50 ps. The SNSPD signals are digitized by commercial time-taggers with timing jitter below 10 ps. A schematic of our network is shown in Fig 11.6.

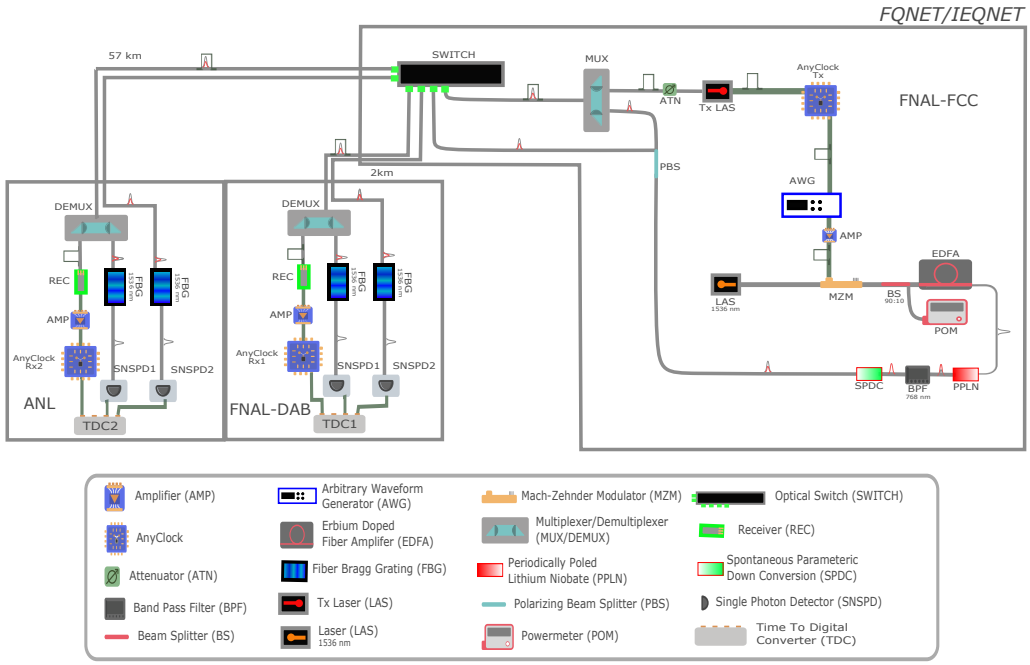

Figure 11.6: Schematic for the FQNET picosecond clock synchronization system. The square pulses represent the clock signal while the grey and red Gaussian-shaped pulses represent the quantum light and its second harmonic (768 nm), respectively. The photon pairs are produced at FNAL-FCC and routed either 2 km away to FNAL-DAB or 57 km away to ANL through software provided with the optical switch [20].

To synchronize the clocks at the FNAL-DAB and ANL nodes with the clock of the central FNAL-FCC node, we implement the system developed in Section 11.2. The transmitter (Tx) module consists of an O- (1310 nm) or L-band (1610 nm) laser diode that is bias switched via 2.5 ns-duration pulses generated by a 200 MHz voltage oscillator. This Tx is used to distribute clock signals from the central FNAL-FCC node to the FNAL-DAB and ANL nodes on the same fiber that is used to transmit the single photons. At the FNAL-DAB and ANL nodes, the receiver (Rx) consists of a 200 MHz-bandwidth photodetector that generates electrical pulses amplified by a custom-designed 15 dB amplifier.These pulses adjust the phase of 200 MHz voltage oscillator clocks at the FNAL-DAB and ANL nodes which are used as time references. The time taggers record the time difference between the electrical signal pulses generated by the SNSPDs and the reference clock signal. The time differences are logged using a scalable data acquisition and monitoring system, enabling uninterrupted quantum network operations.

Results

We characterize the three-node quantum network by measuring the Raman scattering coefficient (see Ref. [21]), timing jitter of the clock distribution system, and coincidence-to-accidental ratio (CAR) of photon pairs distributed from FNAL-FCC to FNAL-DAB and FNAL-FCC to ANL.

We evaluate the drift and timing jitter of the clock synchronization system by monitoring the time difference between the synchronized local clock and a reference signal pulse produced by the same 1536 nm laser that is used for the entangled pair source. The reference signal pulse is modulated by the MZM that is driven by an AWG synchronized with the master clock at the FNAL-FCC central node, and subsequently amplified by the EDFA. This reference signal is transmitted along a fiber parallel to the fiber used to distribute the master clock to the FNAL-DAB and ANL end nodes. At the end nodes, the reference signal is detected by a fast 20 GHz photodetector and digitized by the time tagger. The time difference between the synchronized local clock and the reference signal is collected over each second then plotted in a histogram and long term time drift is monitored through the mean difference, this drift as well as the representative time difference over a period of more than 14 hours can be seen in Figure 11.7.

We observe a drift in the mean of about 3 ps over more than 14 hours and a total jitter of 2.2 ps. This is much less than the 250 ps duration of our photons, which renders our system applicable for quantum networks including those that rely on two-photon interference (e.g., Chapters 8 and 10).

We measure the noise introduced by the clock pulses by measuring the reduction of CAR of our time-correlated photon pairs when they are measured locally at the central FNAL-FCC node compared to when they are distributed over fiber with the clock pulses. From the central FNAL-FCC node, we send to the FNAL-DAB and ANL end nodes the O- and L-band clocks multiplexed along the same fiber that is used to send one of the photons from the correlated pair carrying the quantum signal as described in the previous sections. On a separate fiber parallel to the fiber carrying the multiplexed channel, we send the second photon of the correlated pair. We send clock signals at 0.3 mW power for both the O- and L-bands to the FNAL-DAB end node, while for the ANL end node we send the O-band clock signal at 1.8 mW power and the L-band at 0.3 mW power.

In the absence of Raman scattered photons and dark counts, the CAR is equivalent to the cross-correlation $g^{(2)}(0)$ function, which quantifies the ratio of the detection

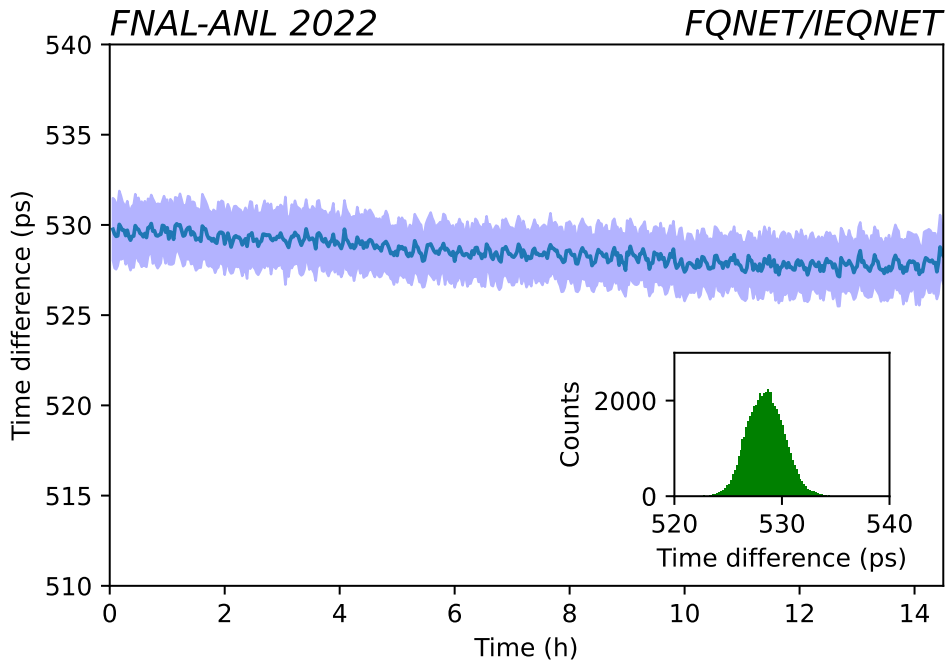

Figure 11.7: Variation of the time difference between the arrival of the reference and derived clock at ANL over 14 hours. The blue line is the average of the time difference every 100 seconds, showing the drift in the time difference of the two clocks. We observe a long term drift of about 3 ps over more than 14 hours, mainly caused by fiber length fluctuations in the link. The blue shaded region is the RMS of the time difference during each of those 100 second intervals. Inset: histogram of the time difference indicates a timing jitter of 2.2 ps.

of correlated photon pairs to non-correlated photon pairs resulting from more than one photon pair being produced at the pair source [12]. We count all photon pair detection events within a 450 ps interval around the main coincidence peak to obtain C, and take the average of the photon pair detection events within a 450 ps interval around each of the accidental peaks to determine A. The measurement is made over a period of 5 minutes for the FNAL-DAB end node. Due to higher losses from the longer distance resulting in lower coincidence rates, it takes 12 hours to make the analogous measurement for the ANL end node.

In Figure 11.8, we show the time difference distribution for the two detected photons in a background-free scenario with the photon pairs sent from the central FNAL-FCC node to the ANL end node and no synchronization clock signal being sent along the same fiber. The main coincidence peak is clearly visible at the center ($\Delta t = 0$),

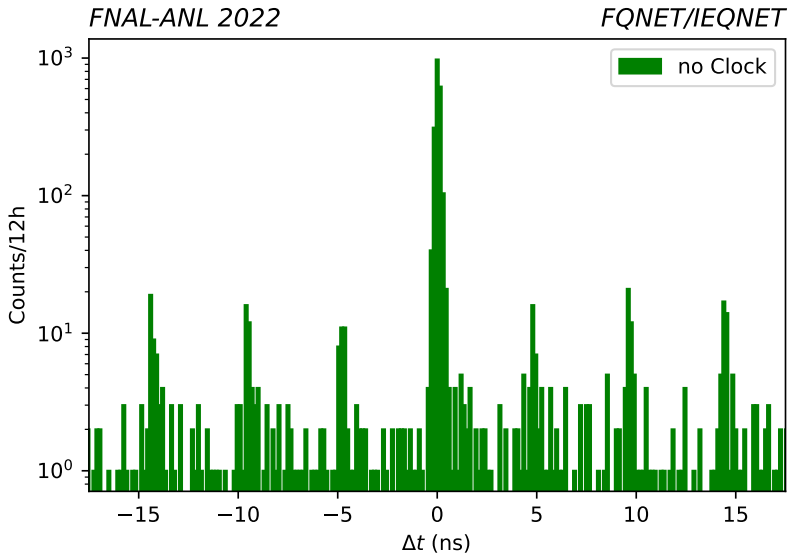

Figure 11.8: Coincidence histogram for the photon pairs sent to ANL from FNAL-FCC with the clock distribution disabled.

and the smaller peaks separated by 5 ns are the "accidental" events corresponding to a detection of one photon from one pair and another photon from preceding or subsequent pairs. We measure a CAR of 51 ± 2 in the background-free scenario.

Next, we sent the photon pairs to the FNAL-DAB and ANL end nodes with the O- and L-band clock synchronization enabled and multiplexed along the same fiber as one of the pairs. The time difference distributions of the two detected photons are shown in Figure 11.9 for the FNAL-DAB and ANL nodes. At the FNAL-DAB end node we measured a CAR of 35 ± 1 with the O-band clock, and 32 ± 1 with the L-band clock. At the ANL end node we measured a CAR of 5.3 ± 0.4 with the O-band clock, and 2.6 ± 0.3 with the L-band clock. The width of the peaks in our measurements are limited by timing jitter in our detectors and readout electronics. We see a reduction in CAR as we increase the length of the fiber, but we stay in the regime where the L-band clock introduces more noise than the O-band clock.

11.4 Discussion and outlook

We have demonstrated a clock-distribution system at the CQNET site for synchronizing remote nodes in metropolitan-scale quantum networks with picosecond-scale resolution. Despite not constituting the optimal choice of wavelength, our telecommunication O-band synchronization system introduces little noise into our telecommunication C-band quantum network. The low noise is partially due to the strong

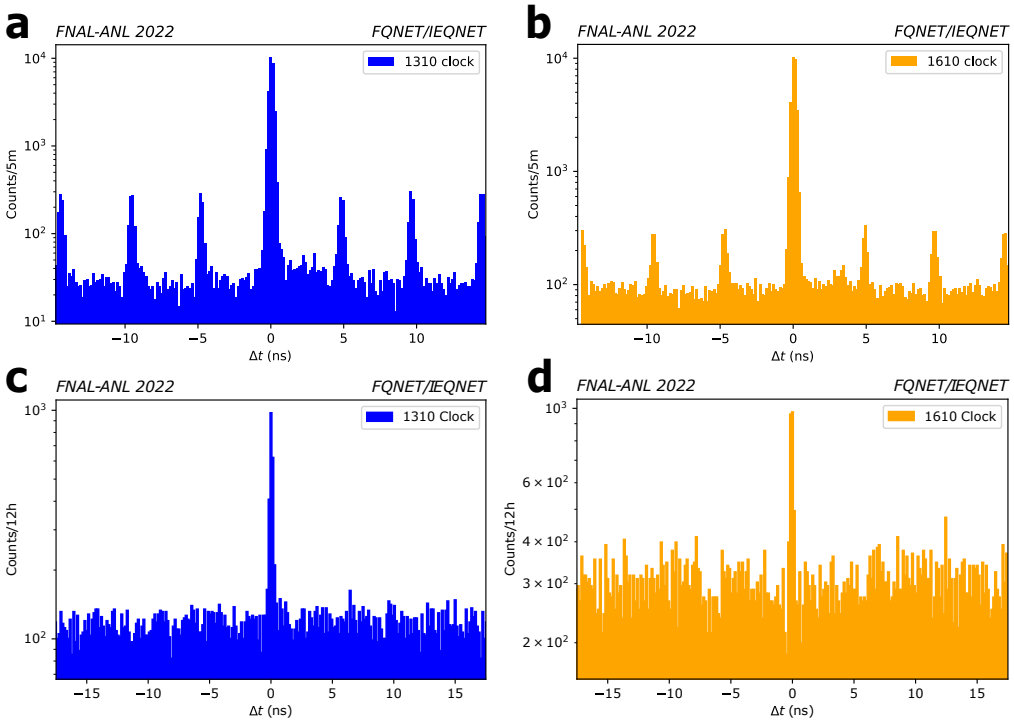

Figure 11.9: Coincidence histograms for the photon pairs sent to FNAL-DAB from FNAL-FCC with the a) 1310 nm and b) 1610 nm clock distribution enabled, and coincidence histograms for the photon pairs sent to ANL from FNAL-FCC with the c) 1310 nm and d) 1610 nm clock distribution enabled.

spectral filtering of the photons at the FBGs – a required step to ensure the photons are purified, i.e., spectral correlations are removed. This renders the photons suitable for two-photon interference, as required for implementations of advanced network protocols, e.g., based on quantum teleportation (Chapters 8 and 10). Note that the 768 nm light remaining after the SPDC step is far off-resonant from the 1536 nm photons, and is partially filtered by the long fiber spools, MUX/DEMUX filters, fiber Bragg gratings, and SNSPD devices, thus it does not contribute any measurable noise to the network. Further reduction of noise in our system can be afforded by detecting the clock pulses with more sensitive REC detectors, thus allowing a reduction of the clock pulse intensity. To this end, SNSPDs operating in the O-band could be used, and would constitute minimal system overhead given that C-band SNSPDs are already deployed. This would also result in improvements to the system clock rate as SNSPDs feature timing jitters as low as a few ps [22], which constitutes an upper-bound of a few hundred GHz to the clock rate (note that the impact of the dead time of the SNSPDs is negligible due to channel loss).

Additionally, we deployed our system over a metropolitan-scale optical fiber network at the FQNET site, demonstrating entanglement distribution with picosecond-level synchronization of remote nodes at FNAL and ANL connected with up to 57 km of optical fiber with timing resolution better than 10 ps. The obtained timing resolution enables quantum sources capable of achieving a repetition rate of the order of 10 GHz, significantly improving the detection rates reported in this study. Furthermore, the clock distribution system can be easily scaled to tens of nodes using very minimal modifications to the current design. We observe that a $CAR > 2.0$, which is above the classical limit, is maintained in all the configurations we tested including using the 57 km installed fiber link between FNAL-FCC and ANL, which has increased losses due to fiber splicing and connectors along the real world fiber connection. Comparing the idealized fiber attenuation loss coefficients in the C-band, our total losses correspond to a transmission of the quantum states over 105 km. Overall, our three-node quantum network and accompanying synchronization system sheds light on the role of noise in quantum networking and constitutes a step towards practical, as well as high-rate, classical-quantum co-existing networks.

References

[1] Akihiro Tanaka, Mikio Fujiwara, Sae Woo Nam, et al. "Ultra fast quantum key distribution over a 97 km installed telecom fiber with wavelength division multiplexing clock synchronization." In: Opt. Express 16.15 (July 2008), pp. 11354–11360. DOI: 10.1364/OE.16.011354.

[2] Yan-Lin Tang, Hua-Lei Yin, Si-Jing Chen, et al. "Field Test of Measurement-Device-Independent Quantum Key Distribution." In: IEEE Journal of Selected Topics in Quantum Electronics 21.3 (2015), pp. 116–122. DOI: 10.1109/JSTQE.2014.2361796.

[3] Raju Valivarthi, Marcelli Grimau Puigibert, Qiang Zhou, Gabriel H Aguilar, Varun B Verma, Francesco Marsili, Matthew D Shaw, Sae Woo Nam, Daniel Oblak, and Wolfgang Tittel. "Quantum teleportation across a metropolitan fibre network." In: Nature Photonics 10.10 (2016), pp. 676–680.

[4] Qi-Chao Sun, Ya-Li Mao, Si-Jing Chen, Wei Zhang, Yang-Fan Jiang, Yan-Bao Zhang, Wei-Jun Zhang, Shigehito Miki, Taro Yamashita, Hirotaka Terai, et al. "Quantum teleportation with independent sources and prior entanglement distribution over a network." In: Nature Photonics 10.10 (2016), pp. 671–675.

[5] Raju Valivarthi, Prathwiraj Umesh, Caleb John, Kimberley A Owen, Varun B Verma, Sae Woo Nam, Daniel Oblak, Qiang Zhou, and Wolfgang Tittel. "Measurement-device-independent quantum key distribution coexisting with classical communication." In: Quantum Science and Technology 4.4 (2019), p. 045002.

[6] James Williams, Martin Suchara, Tian Zhong, Hong Qiao, Rajkumar Kettimuthu, and Rikuto Fukumori. "Implementation of quantum key distribution and quantum clock synchronization via time bin encoding." In: Quantum Computing, Communication, and Simulation. Ed. by Philip R. Hemmer and Alan L. Migdall. Vol. 11699. International Society for Optics and Photonics. SPIE, 2021, pp. 16–25. DOI: 10.1117/12.2581862.

[7] Iris Choi, Robert J. Young, and Paul D. Townsend. "Quantum key distribution on a 10Gb/s WDM-PON." In: Opt. Express 18.9 (Apr. 2010), pp. 9600–9612. DOI: 10.1364/OE.18.009600.

[8] KA Patel, JF Dynes, I Choi, AW Sharpe, AR Dixon, ZL Yuan, RV Penty, and AJ Shields. "Coexistence of high-bit-rate quantum key distribution and data on optical fiber." In: Physical Review X 2.4 (2012), p. 041010.

[9] DOE's Quantum Internet Blueprint. https://www.energy.gov/sites/prod/files/2020/07/f76/QuantumWkshpRpt20FINAL_Nav_0.pdf.

[10] Tektronix. https://www.tek.com/en/products/arbitrary-waveform-generators/. Accessed: 2022-03-09.

[11] Shf. https://www.shf-communication.com/products/rf-broadband-amplifiers/. Accessed: 2022-03-09.

[12] Rodney Loudon. The quantum theory of light. Oxford, 2000.

[13] I. Marcikic, H. de Riedmatten, W. Tittel, V. Scarani, H. Zbinden, and N. Gisin. "Time-bin entangled qubits for quantum communication created by femtosecond pulses." In: Phys. Rev. A 66 (6 Dec. 2002), p. 062308. DOI: 10.1103/PhysRevA.66.062308.

[14] Hiroki Takesue and Kyo Inoue. "1.5-μm band quantum-correlated photon pair generation in dispersion-shifted fiber: suppression of noise photons by cooling fiber." In: Opt. Express 13.20 (Oct. 2005), pp. 7832–7839. DOI: 10.1364/OPEX.13.007832.

[15] Hiroki Takesue and Kyo Inoue. "Generation of 1.5$-\mu$m band time-bin entanglement using spontaneous fiber four-wave mixing and planar light-wave circuit interferometers." In: Phys. Rev. A 72 (4 Oct. 2005), p. 041804. DOI: 10.1103/PhysRevA.72.041804.

[16] Reinhard F. Werner. "Quantum states with Einstein-Podolsky-Rosen correlations admitting a hidden-variable model." In: Phys. Rev. A 40 (8 Oct. 1989), pp. 4277–4281. DOI: 10.1103/PhysRevA.40.4277. URL: https://link.aps.org/doi/10.1103/PhysRevA.40.4277.

[17] John F. Clauser, Michael A. Horne, Abner Shimony, and Richard A. Holt. "Proposed Experiment to Test Local Hidden-Variable Theories." In: Phys. Rev. Lett. 23 (15 Oct. 1969), pp. 880–884. DOI: 10.1103/PhysRevLett.23.880.

[18] Home: QuTag. https://www.qutools.com/qutag/. URL: https://www.qutools.com/qutag/.

[19] IxBlue. https://www.ixblue.com/north-america/store/dr-ve-10-mo/.

[20] Polatis. https://www.polatis.com/series_6000_multimode_switch_all-optical_switching.asp.

[21] Keshav Kapoor, Si Xie, Joaquin Chung, Raju Valivarthi, Cristián Peña, Lautaro Narváez, Neil Sinclair, Jason P. Allmaras, Andrew D. Beyer, Samantha I. Davis, et al. "Picosecond synchronization system for the distribution of photon pairs through a fiber link between Fermilab and Argonne National Laboratories." In: IEEE Journal of Quantum Electronics 59.4 (2023), pp. 1–7.

[22] Boris Korzh, Qing-Yuan Zhao, Jason P. Allmaras, et al. "Demonstration of sub-3 ps temporal resolution with a superconducting nanowire single-photon detector." In: Nature Photonics 14.4 (Apr. 2020), pp. 250–255. ISSN: 1749-4893. DOI: 10.1038/s41566-020-0589-x.